







Article

Seasonal Variability in the Composition of Particulate Matter and the Microclimate in Cultural Heritage Areas

Cristiana Radulescu ^{1,2,*} , Claudia Stihl ^{1,2,*} , Rodica-Mariana Ion ^{3,4} , Ioana-Daniela Dulama ², Sorina-Geanina Stanescu ² , Raluca Maria Stirbescu ², Sofia Teodorescu ², Ion-Valentin Gurgu ², Dorin-Dacian Let ², Liviu Olteanu ², Nicolae-Mihail Stirbescu ², Ioan-Alin Bucurica ² , Radu-Lucian Olteanu ² and Cristina-Mihaela Nicolescu ² 

¹ Faculty of Sciences and Arts, Valahia University of Targoviste, 130004 Targoviste, Romania

² Institute of Multidisciplinary Research for Science and Technology, Valahia University of Targoviste, 130004 Targoviste, Romania; dulama_id@yahoo.com (I.-D.D.); geaninastanescu@yahoo.com (S.-G.S.); stirbescu_nic@yahoo.com (R.M.S.); sofiateodorescu@yahoo.com (S.T.); gurguvalentin@gmail.com (I.-V.G.); ldorin@icstm.ro (D.-D.L.); liviu.olteanu@gmail.com (L.O.); nicolaestirbescu@yahoo.com (N.-M.S.); bucurica_alin@yahoo.com (I.-A.B.); raduolteanu110@yahoo.com (R.-L.O.); cristina.nicolescu.profa@gmail.com (C.-M.N.)

³ Faculty of Materials Engineering and Mechanics, Valahia University of Targoviste, 130004 Targoviste, Romania; rodica_ion2000@yahoo.co.uk

⁴ National Institute of Research and Development for Chemistry and Petrochemistry—ICECHIM, 060021 Bucharest, Romania

* Correspondence: radulescucristiana@yahoo.com (C.R.); claudia.stihl@valahia.ro (C.S.)

Received: 29 August 2019; Accepted: 30 September 2019; Published: 2 October 2019



Abstract: This study is the first attempt to decipher the effect of particulate matter (PM) composition on people's health and on historic sites, in correlation with the daily and seasonal microclimate monitoring of the indoor and outdoor areas of the Roman Mosaic Edifice museum (the maritime port of Constanta, Romania). More specifically, the increase of metal concentrations in particulate matter during the summer of 2018 and spring of 2019 in the museum under investigation could possibly be associated with the microclimates of both seasons, with coastal factors, as well as with the anthropic activities specific to the port of Constanta. FTIR and inductively coupled plasma mass spectroscopy (ICP-MS) techniques, used for the investigation of PM_{2.5–10} samples, revealed high concentrations of Fe, Al-rich, and soluble particles inside the investigated museum area. In this respect, the chemical measurements of the PM_{2.5–10} masses highlighted high concentrations of heavy metals (i.e., Al, Fe, Zn, Mn, and Pb) and low concentrations of trace metals (i.e., Cr, Ni, Cu, and Cd). Statistical analysis showed that the chemical compositions of the particulate matter in the indoor and outdoor areas of the Roman Mosaic Edifice were influenced by microclimatic conditions, mainly temperature and relative humidity (RH). A potential health risk for tourists is the thermal and humid conditions, alongside the toxic components of the particulate matter. This research seeks to provide solutions for improving the environmental conditions inside the Roman Mosaic Edifice and to offer useful suggestions concerning health promotion and the protection of museum exhibits against possible future deterioration.

Keywords: particulate matter; microclimate; museum; health promotion; FTIR; ICP-MS; statistical analysis

1. Introduction

Air quality (indoor and outdoor) is considered to be one of the main issues related to people's health [1–5]. Long-term exposure to a high or even low concentrations of particulate matter (PM) and soot particles can cause cancer and premature death, according to the World Health Organization (WHO) Air quality guidelines (AQGs), in which possible concentrations of PM_{2.5} as 10 µg/m³ annual mean and 25 µg/m³ as 24-h mean as well as for PM₁₀ values of 20 µg/m³ annual mean and 50 µg/m³ 24-h mean are recommended [6]. Also, it has been reported that long-term exposure to PM_{2.5} is associated with an increase in cardiopulmonary mortality by 6–13% for 10 µg/m³ PM_{2.5} [7,8]. Health outcomes have been associated with long-term exposure to particulate matter, with respiratory illness leading in children under five years of age and chronic obstructive pulmonary disease (COPD), ischemic heart disease (IHD), stroke, and lung cancers in adults [6]. Other substances, such as carbon oxides (CO_x), nitrogen oxides (NO_x) and sulfur dioxide (SO₂), and volatile organic compounds (VOCs) are considered to belong in the first category of pollutants, with harmful effects on both people's health and the environment [9]. Gaseous oxides in the atmosphere, such as sulfur and nitrogen oxides (SO₂ and NO_x), react with water molecules, thus resulting in sulfuric acid and nitric acid, respectively (well-known as acid rain), with damaging effects on plants, aquatic animals, and the infrastructure [10–13]. According to Camuffo et al., atmospheric pollution is a serious problem for historical artefacts (e.g., surface alteration, color change, or even weakening of the original structure of the material), especially for vulnerable and sensitive materials of high cultural value, as are found in museums [14]. Several studies have shown that air pollutants can have a damaging effect not only on historical artefacts and art objects in museums, but also on tourists [15,16]. According to other studies, it was demonstrated that some tourists perceive the PM inside a museum as posing potential health risks [3–5,17]. Over the years, researchers have reported different results regarding the conditions for the rehabilitation of cultural heritage sites, highlighting that special attention needs to be paid to indoor/outdoor control of the microclimate, in view of the preservation of cultural heritage areas [14,18–20]. Therefore, the microclimate plays an important role in the deterioration process of historical material. In this respect, original art collections, sensitive to high levels of ambient temperature and relative humidity (RH), need to be displayed or stored inside the museums in observance of all the requirements regarding their proper storage and protection for a historical period. Daily and seasonal cycles in temperature and RH induce changes in the material content, due to the occurrence of chemical reactions and biological species (i.e., molds, plants, and insects) [21]. The synergism between pollutants (e.g., gaseous oxides, PM, VOCs, etc.), temperature, and humidity can deteriorate objects of art; sometimes the results can be irreversibly destructive [22]. The chemical composition of PM is linked mainly to the presence of trace elements (i.e., Ag, As, Ba, Be, Dc, Ce, Cr, Co, Cu, Fe, Mn, Nd, Ni, Pb, Sb, Se, Sr, Ti, V, and Zn) in oxides or inorganic salts (e.g., sulfate, sulfide, nitrate, carbonate, silicate, and chloride), water, organic substances, black carbon, mineral dust and other components in the Earth's crust, as well as low concentrations of various species, including bioactive organic compounds and redox cycling metals [5,23–25]. According to Spolnik et al., there are some possible direct processes through which sulfate and nitrate anions from PM, correlated with high temperature, may affect heritage-related endpoints, including interactions with some metals [25]. Further free radicals such as SO₂· and irritant peroxyacetyl nitrates (PANs) are dangerous to people's health and to materials [26]. The deposition of PM inside museums strongly depends on particle size and is governed by the processes of particle diffusion onto the surface of old structures, which is of particular significance for small particles (PM less than 10 µm in size), and of gravitational sedimentation, which is significant for larger particles (PM higher than 10 µm in size) [27].

In Black Sea countries such as Romania, microclimatic factors such as high temperature, high humidity, solar radiation, and coastal conditions are strongly correlated with photochemical air pollutants (i.e., ozone and other oxidizing compounds, such as hydrogen peroxide, aldehydes, and PANs) and tourism development, thus becoming a significant issue concerning cultural heritage rehabilitation [28]. In the historical area of Constanta (Romania), on the western coast of the Black

Sea, 179 km from the Bosphorus Strait, there are several museums located in old buildings with natural ventilation, low heating and natural luminosity, high humidity, and often with a moldy smell. The safety of the museum environment in relation to the inside air quality, with its direct consequences on exhibited collections and on visitor's health, involves the development of new strategies for indoor/outdoor air pollution restrictions and of new rehabilitation procedures for old buildings.

The Roman Mosaic Edifice is located near the Museum of National History and Archaeology and was discovered in 1959, being part of the ancient town of Tomis (present-day Constanta) [29]. Further research discovered that the monument was built in the fourth century and was gradually expanded until around the sixth century, when the construction work stopped. In its times of glory, the edifice represented the largest building of its kind in the whole Roman Empire and served as a link between the port and the ancient city, the place where it conducted its trade and secured the storage of goods. Originally, the building spanned three of the four terraces of the ancient Tomis harbor waterfront [29]. After the fall of the Tomis fortress in the sixth century, the building fell into decay. However, the high-quality mosaic of the floor has been very well preserved. At present, from a total area of 2000 square meters of mosaic pavement, only a portion of about 850 square meters has been preserved [27]. The floor is of a unique beauty and consists of two distinct parts: a framework, which borders the room perimeter, and the vegetal and geometric patterns of the mosaic itself, which is made up of pebbles of different colors including white, red, yellow, green, and black [29]. Unfortunately, the premises hosting the Roman Mosaic Edifice are improper for storage and visiting purposes. This place is built on a metal structure with large windows, natural ventilation, very high temperatures and humidity during the warmer season, and no heating during the rainy and cold seasons. It is located about two kilometers away from the sea port of Constanta, the main port in the Black Sea, the most important one in Romania, and the fourth most important in Europe.

These environmental conditions (indoor and outdoor) can significantly influence the degradation processes of the materials and components of the Roman Mosaic. The air temperature and relative humidity are key variables of research in the field of environmental protection. Both parameters are hard to monitor, especially at a national scale, due to spatial heterogeneity. The temperature is expected to increase in the course of this century, and extreme values (53.7 °C) were recorded in 2017. The variations in the minimum and maximum temperatures recorded are the main factors that impact the degradation process of the original materials. It is well-known that organic and inorganic materials are extremely sensitive to thermo-hygrometric cycles, especially to shorter ones (i.e., daily cycles, with repeated dilatations/contractions), because they generate steep gradients starting from the outer surface of the object and giving rise to inner tensions, which result in dimensional variations and may lead to irreversible changes in the chemical composition of the original materials.

A potential health risk for visitors is the thermal and humid conditions, together with the toxic components of the particulate matter. Due to climate change and the potential changes in ambient temperatures and RH, it is essential that we seek a better understanding of the indoor thermal conditions and of the air quality in cultural heritage areas.

This research is the first attempt to decipher the effect of PM composition on public health and historical artefacts, in correlation with the monitoring of the daily and seasonal microclimate inside and outside the Roman Mosaic Edifice area. The aim of this study was to investigate the indoor and outdoor conditions of the Roman Mosaic Edifice by several parameters: temperature, apparent temperature (AT), relative humidity (RH), and particulate matter composition. The novelty of this study is highlighted by the multitude of reported data (indoor and outdoor) with direct correlations between climatic factors and PM chemical composition, which has a direct influence on artwork in the museum and on visitor's health.

This research seeks to provide solutions for improving the environmental conditions inside the Roman Mosaic Edifice area and identify useful ways to promote the health safety of visitors and to protect the museum exhibits against possible future deterioration.

2. Methodology

This research presents the results of an in-field experimental campaign carried out by means of noninvasive measuring instruments, such as a PCE FWS20 weather station and a TE-Wilbur low-volume air particulate matter sampler, equipped with polytetrafluoroethylene (PTFE) filters ($d = 0.45 \mu\text{m}$, $\Phi = 47 \text{ mm}$) for particle sampling. These filters were chosen so that a relatively clean IR absorbance spectrum would be obtained [5,24]. The monitoring campaign was undertaken during four seasons—the summer, autumn, and winter of 2018 and the spring of 2019. The measurements and samplings were performed for 24 h/d, 7 d/week, for every month in the risk period (very warm months and rainy, cold months), also taking into account the meteorological predictions provided by the National Meteorological Administration (INMH). A total of 84 filter samples were collected for the purpose of chemical composition examination.

2.1. Temperature, Relative Humidity, and Apparent Temperature Investigations

Temperature (T) and relative humidity (RH) measurements were performed by using the PCE FWS20 weather station, with an accuracy of $\pm 0.5\%$ from -25 to 70°C for temperature and $\pm 2.5\%$ from 11% to 90% for RH. The temperature and RH measurements were used in order to determine the indoor and outdoor thermal conditions. The apparent temperature, the temperature felt by people, was calculated according to the equation [30]:

$$AT = -2.65 + (0.99 \times T)(0.01 \times T_d^2), \quad (1)$$

where T is the mean temperature, and T_d is the dewpoint temperature measured together with the temperature values.

2.2. $\text{PM}_{2.5-10}$ Sample Analysis

Molecular investigation of the functional groups of inorganic and organic compounds deposited on filters was performed by attenuated total reflection Fourier transform infrared spectroscopy (ATR-FTIR) (Bruker, Wetzlar, Germany), using a Vertex 80v spectrometer (Bruker, Wetzlar, Germany) equipped with diamond ATR crystal accessory for highly refractive index bulk samples, as well as by a Hyperion microscope (Bruker, Wetzlar, Germany). ATR-FTIR spectroscopy has limited applications in quantitative research, since it has a penetration depth of only a few microns, but for qualitative investigation it could be a suitable technique. The ATR-FTIR method did not require a special preparation of samples. The blank was handled exactly as each sample filter from the pre-scan until the final analysis was completed. The samples were chosen based on their black color and thickness ($\sim 2 \text{ mm}$) and were placed into 47 mm Petri dishes. The “thick” spectra (recorded from seven samples/season of PM collected on filter) were analyzed in the range of $4000\text{--}400 \text{ cm}^{-1}$ (being representative for what can generally be obtained from $\text{PM}_{2.5-10}$ particles) by non-destructive transmission FTIR spectroscopy.

The concentrations of Al, Cr, Mn, Fe, Ni, Cu, Zn, Cd, and Pb in $\text{PM}_{2.5-10}$ samples were determined by inductively coupled plasma mass spectroscopy (ICP-MS), using an iCAPTM Qc device (Thermo Scientific, Bremen, Germany). The optimal instrumental parameters and detection limits for the elements analyzed are presented in Table 1. The samples were digested in HNO_3 on a hot plate by using a TOPwave microwave-assisted pressure system (Analytik Jena, Munich, Germany). All chemical reagents were of analytical grade. The measurements were performed in triplicate. The standard reference material (i.e., NIST SRM 1648a, Urban Particulate Matter) was used to verify the accuracy and traceability of the method. The relative standard deviation (RSD) of the standard was 0.36%, the RSD of the samples was 1.2–2.4%, and the recovery of the elements ranged between 92.5% and 104.8%.

Table 1. Inductively coupled plasma mass spectroscopy (ICP-MS) instrumental parameters and detection limits for determined metals.

Optimal Instrumental Parameters	Metals Detection Limit ($\mu\text{g/kg}$)
Plasma Power: 1548.6 W	Al: 16.51 Cr: 1.50 Mn: 0.48
Nebulizer Ar flow: 1 L/min	Fe: 4.31 Ni: 0.73 Cu: 1.19
Plasma Ar flow: 10.75 L/min	Cu: 1.19 Zn: 8.92 Cd: 0.13
Sample uptake rate: 0.4 mL/min	Pb: 1.23

2.3. Statistical Analysis

Statistical analysis was performed using Statistical Package for the Social Science (SPSS) software v.24.0 for MS Windows in order to obtain the Pearson correlations between element concentrations and microclimate parameters [31–34]. The relationship between outdoor and indoor temperature was determined by a linear regression model.

3. Results and Discussion

3.1. Temperature, Relative Humidity, and Apparent Temperature

The results of the descriptive statistical analysis of temperature, RH, and AT from the Roman Mosaic Edifice for indoor and outdoor areas in different seasons are shown in Table 2.

Table 2. Descriptive statistics of temperature, relative humidity (RH) and apparent temperature (AT) from the Roman Mosaic Edifice area comparative to reported data [35].

Season	Parameter	Minimum	Maximum	Mean	Median	Standard Deviation	Reported Data [35]
Summer	Indoor						
	T [$^{\circ}\text{C}$]	27.00	31.70	29.17	28.90	1.00	21.07
	RH [%]	46.60	62.60	53.81	54.60	4.83	62.67
	AT [$^{\circ}\text{C}$]	29.56	34.21	31.71	31.44	3.04	-
	Outdoor						
	T [$^{\circ}\text{C}$]	25.10	38.20	29.11	28.40	2.78	-
Autumn	RH [%]	28.00	70.00	47.28	48.00	8.80	-
	AT [$^{\circ}\text{C}$]	27.67	40.64	31.64	30.94	2.25	-
	Indoor						
	T [$^{\circ}\text{C}$]	11.40	16.40	13.93	13.90	1.25	10.67
	RH [%]	43.00	53.00	48.48	49.00	7.39	72.33
	AT [$^{\circ}\text{C}$]	13.97	18.92	16.48	16.45	2.15	-
Winter	Outdoor						
	T [$^{\circ}\text{C}$]	0.70	5.40	3.27	3.00	1.35	-
	RH [%]	72.00	99.00	91.90	94.00	6.55	-
	AT [$^{\circ}\text{C}$]	3.36	8.02	5.91	5.64	1.06	-
	Indoor						
	T [$^{\circ}\text{C}$]	5.80	14.90	9.87	9.50	2.31	-1.73
Winter	RH [%]	53.00	68.60	60.03	61.05	3.10	74
	AT [$^{\circ}\text{C}$]	8.43	17.44	12.46	12.09	1.35	-
	Outdoor						
	T [$^{\circ}\text{C}$]	2.10	18.10	10.38	10.40	4.07	-
Winter	RH [%]	30.00	84.00	57.20	57.00	12.38	-
	AT [$^{\circ}\text{C}$]	4.74	20.58	12.94	12.96	1.72	-

Table 2. Cont.

Season	Parameter	Minimum	Maximum	Mean	Median	Standard Deviation	Reported Data [35]
Spring	Indoor						
	T [°C]	22.50	26.30	24.96	25.00	0.64	9.66
	RH [%]	52.10	63.50	58.91	59.10	2.45	68.66
	AT [°C]	25.09	28.85	27.53	27.57	3.17	-
	Outdoor						
	T [°C]	20.30	30.20	25.58	25.30	1.98	-
	RH [%]	26.00	99.00	42.81	42.00	12.65	-
	AT [°C]	22.86	32.66	28.09	27.81	4.05	-

Indoor and outdoor temperature and AT values showed a seasonal pattern with high values during the summer of 2018 and low values in the autumn and winter of 2018 (Figure 1).

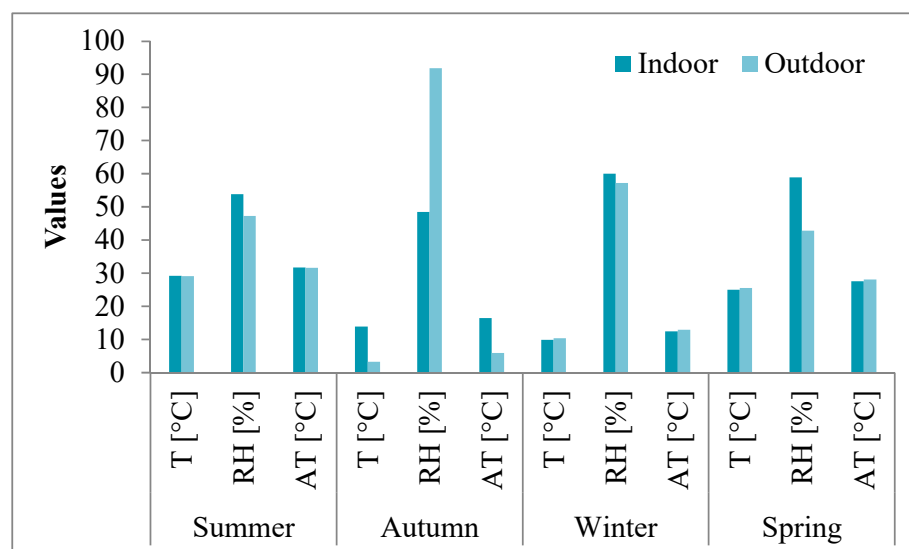


Figure 1. Seasonal mean values of indoor and outdoor temperature, RH, and AT.

Regarding the RH, high values were recorded in the autumn of 2018 inside the Roman Mosaic Edifice area, where the maximum recommended value for human comfort was exceeded. High outdoor humidity and low outdoor temperatures were measured in the autumn season, and in that case the air felt as chilly as in winter [36].

The mean thermal humidity index (MTHI) was calculated for each season using the Formula (2) [37]:

$$\text{MTHI} = 0.81 \times T + 0.01 \times \text{RH} \times (0.99 \times T - 14.3) + 46.3, \quad (2)$$

where T and RH are the mean values of temperature and RH.

According to the MTHI obtained, the thermal comfort status of the visitor was recorded in the autumn and winter seasons, both indoors (57.33 and 51.57) and outdoors (38.78 and 52.40) of the Roman Mosaic Edifice. For the summer and spring seasons, a high thermal comfort status was registered for both the indoor (77.77 and 72.65) and outdoor areas (76.74 and 71.73) of the Roman Mosaic Edifice. No thermal discomfort conditions were recorded in any season. The relationship between outdoor and indoor temperature is shown in Figure 2. Through a linear regression model, a strong correlation was detected between the average outdoor and indoor temperatures ($r = 0.90$, $b = 0.69$).

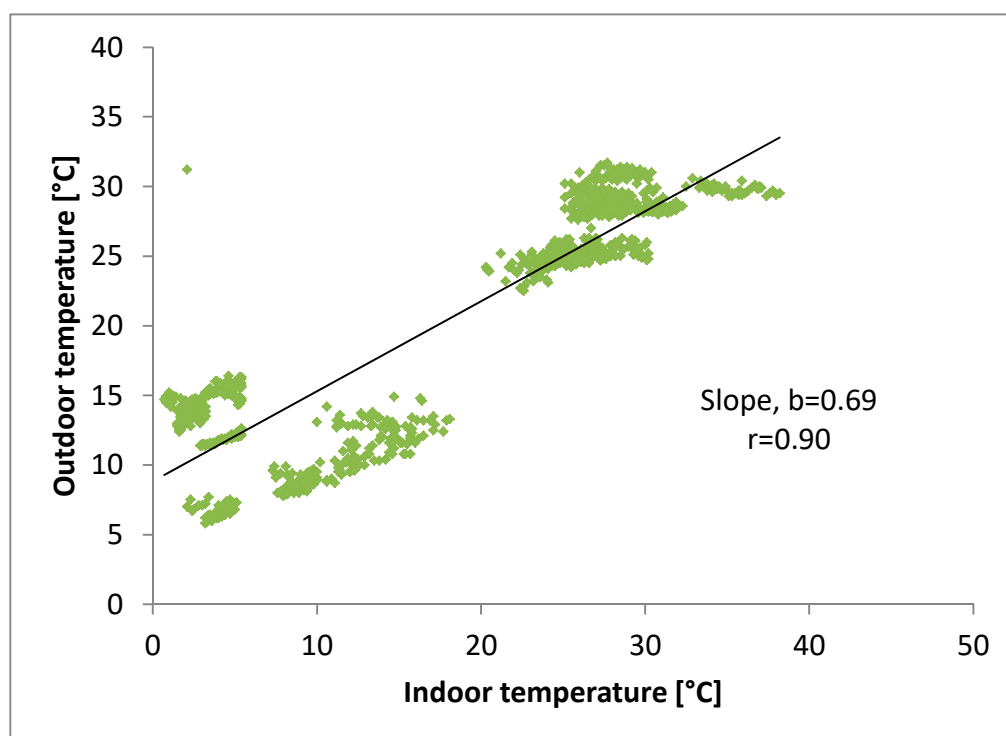


Figure 2. Regression results for the outdoor and indoor temperature.

3.2. $PM_{2.5-10}$ Metal Composition

The results of the descriptive statistics analysis of Al, Cr, Mn, Fe, Ni, Cu, Zn, Cd, and Pb concentrations in $PM_{2.5-10}$ collected from the indoor and outdoor area of the Roman Mosaic Edifice are presented in Tables 3 and 4.

Table 3. Descriptive statistics of metal concentrations in $PM_{2.5-10}$ samples ($N = 84$) collected in the summer and autumn seasons of 2018 [mg/kg].

Season	Metals	Minimum	Maximum	Mean	Median	Standard Deviation	Coefficient of Variation (%)	
Summer	Indoor	Al	3.09	4.15	3.56	3.3	0.55	15.45
		Cr	0.72	1.52	0.99	0.87	0.32	32.32
		Mn	1.36	1.91	1.71	1.79	2.09	1.22
		Fe	8.09	9.67	8.95	8.75	2.53	28.27
		Ni	4.9	6.07	5.3	5.11	0.47	8.87
		Cu	5.22	6.82	5.88	5.43	0.72	12.24
		Zn	3.61	6.74	5.71	6.06	1.26	22.07
		Cd	0.64	0.96	0.79	0.75	0.12	15.19
		Pb	4.58	5.43	5.03	5.11	0.34	6.76
	Outdoor	Al	4.15	5.86	4.58	4.37	0.72	15.72
		Cr	1.72	3.09	2.42	2.45	0.67	27.69
		Mn	20.88	25.35	23.73	24.18	1.8	7.59
		Fe	99.92	114.83	107.74	110.57	6.79	6.30
		Ni	7.99	10.44	9.03	9.05	0.96	10.63
		Cu	8.1	9.69	8.99	9.37	0.74	8.23
		Zn	76.59	95.76	86.99	88.2	7.01	8.06
Cd		0.96	1.28	1.17	1.17	0.13	11.11	
Pb		6.18	7.24	6.56	6.5	0.42	6.40	

Table 3. Cont.

Season	Metals	Minimum	Maximum	Mean	Median	Standard Deviation	Coefficient of Variation (%)	
Autumn	Indoor	Al	1.44	1.93	1.65	1.53	0.21	12.73
		Cr	0.18	0.38	0.25	0.21	0.09	36.00
		Mn	3.3	4.62	4.14	4.34	0.56	13.53
		Fe	6.46	7.72	7.15	6.99	0.52	7.27
		Ni	0.81	1.01	0.88	0.85	0.09	10.23
		Cu	0.75	0.98	0.84	0.78	0.11	13.10
		Zn	3.99	7.47	6.32	6.71	1.49	23.58
		Cd	0.05	0.09	0.06	0.06	0.01	16.67
		Pb	0.37	0.44	0.4	0.42	0.03	7.50
	Outdoor	Al	2.39	3.37	2.63	2.5	0.44	16.73
		Cr	0.22	0.4	0.32	0.32	0.07	21.88
		Mn	4.54	5.51	5.16	5.25	0.42	8.14
		Fe	6.6	7.6	7.13	7.31	0.42	5.89
		Ni	1.32	1.74	1.5	1.5	0.17	11.33
		Cu	1.36	1.64	1.52	1.59	0.12	7.89
		Zn	6.22	7.79	7.07	7.17	0.64	9.05
Cd		0.11	0.15	0.14	0.14	0.01	7.14	
Pb		0.63	0.75	0.67	0.66	0.04	5.97	

Table 4. Descriptive statistics of metal concentrations in PM_{2.5–10} samples (N = 84) collected in the winter and spring seasons of 2019 [mg/kg].

Season	Metals	Minimum	Maximum	Mean	Median	Standard Deviation	Coefficient of Variation (%)	
Winter	Indoor	Al	1.02	1.36	1.17	1.08	0.15	12.82
		Cr	0.13	0.27	0.17	0.15	0.06	35.29
		Mn	2.33	3.26	2.93	3.06	0.4	13.65
		Fe	4.56	5.45	5.05	4.93	0.37	7.33
		Ni	0.57	0.71	0.62	0.6	0.06	9.68
		Cu	0.53	0.69	0.59	0.55	0.08	13.56
		Zn	2.82	5.27	4.46	4.74	1.05	23.54
		Cd	0.04	0.06	0.05	0.05	0.01	20.00
	Pb	0.26	0.31	0.29	0.29	0.02	6.90	
	Outdoor	Al	1.68	2.38	1.86	1.77	0.31	16.67
		Cr	0.16	0.29	0.23	0.23	0.05	21.74
		Mn	3.2	3.89	3.64	3.71	0.29	7.97
		Fe	4.66	5.36	5.03	5.16	0.29	5.77
		Ni	0.93	1.23	1.06	1.06	0.12	11.32
		Cu	0.96	1.16	1.08	1.12	0.08	7.41
		Zn	4.39	5.5	4.99	5.06	0.45	9.02
Cd		0.08	0.11	0.1	0.1	0.01	10.00	
Pb	0.44	0.53	0.47	0.47	0.03	6.38		
Spring	Indoor	Al	1.6	2.15	1.84	1.71	0.29	15.76
		Cr	0.38	0.79	0.51	0.45	0.17	33.33
		Mn	7.07	9.88	8.86	9.28	1.08	12.19
		Fe	4.19	5.01	4.64	4.53	3.38	72.84
		Ni	2.54	3.15	2.75	2.65	0.24	8.73
		Cu	2.71	3.53	3.05	2.82	0.38	12.46
		Zn	8.72	14.95	9.6	11.42	6.55	78.23
		Cd	0.33	0.5	0.41	0.39	0.06	14.63
	Pb	2.37	2.82	2.61	2.65	0.18	6.90	
	Outdoor	Al	2.15	3.04	2.37	2.26	0.38	16.03
		Cr	0.89	1.6	1.25	1.27	0.35	28.00
		Mn	10.82	13.14	12.3	12.53	0.93	7.56
		Fe	51.79	59.52	55.85	57.32	3.52	6.30
		Ni	4.14	5.41	4.68	4.69	0.5	10.68
		Cu	4.2	5.02	4.66	4.86	0.38	8.15
		Zn	39.7	49.64	45.09	45.72	3.63	8.05
Cd		0.5	0.66	0.61	0.61	0.07	11.48	
Pb	3.2	3.75	3.4	3.37	0.22	6.47		

The order of the metals present, corresponding to their abundance in the PM_{2.5–10} samples from the indoor area of the Roman Mosaic Edifice, was: Cd < Cr < Mn < Al < Pb < Ni < Zn < Cu < Fe in the summer season; Cd < Cr < Pb < Cu < Ni < Al < Mn < Zn < Fe in the autumn and winter seasons; and Cd < Cr < Al < Pb < Ni < Cu < Cu < Fe < Mn < Zn in the spring season. The order of the metals present, in terms of their abundance in the PM_{2.5–10} samples from the outdoor area of the Roman Mosaic Edifice was: Cd < Cr < Al < Pb < Cu < Ni < Mn < Zn < Fe in the summer and spring seasons and Cd < Cr < Pb < Ni < Cu < Al < Mn < Zn < Fe in the autumn and winter seasons. It can be noticed

that in the autumn season, the order of the metals was the same in both the indoor and outdoor areas. A high value of the coefficient of variation (CV), defined as the ratio of the standard deviation to the mean values, was found for Zn (78.73) and Fe (72.84) in the indoor samples collected in the spring seasons. There was a moderate variation in the concentration of Cr ($25\% < CV < 50\%$) in the indoor samples collected in all the seasons and in the outdoor samples collected in the summer season as well. There was also a moderate variation in the concentration of Fe (28.27%) in the indoor samples collected in the summer season. Except for the abovementioned situations, a weak variability ($CV < 25\%$) was found for all the metals.

From data reported in Tables 3 and 4, the indoor and outdoor (I/O) ratio was calculated, and the obtained results are presented more clearly in the following graph (Figure 3). In this respect, two types of observations can be reported: the first group of metals (i.e., Al, Cu, Cd, and Pb) showed high ratios in summer and spring seasons, while the second group of metals (i.e., Cr, Mn, Fe, and Zn) showed high ratios in autumn and winter seasons. This can be explained by the high level of metal pollution in warm seasons, while in cold seasons, the metal content in PM (outdoor) decreased. The Ni was a singular case, and the I/O ratio was constant throughout the entire monitoring process.

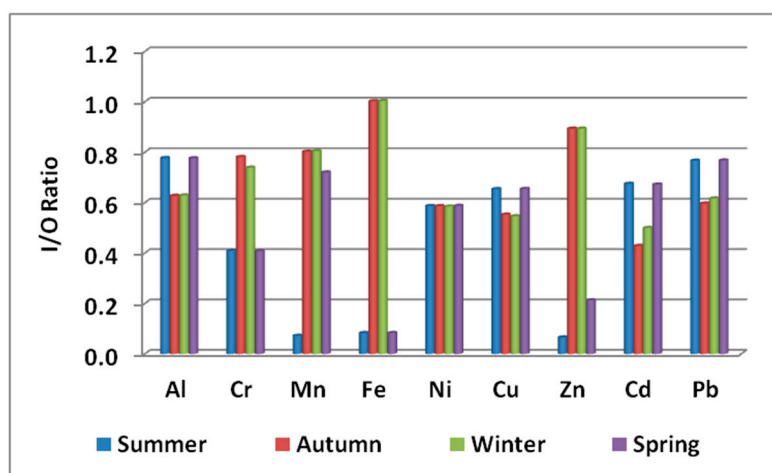


Figure 3. Ratio between indoor and outdoor (I/O) metal concentrations in PM_{2.5-10} samples.

High concentrations of Pb were found in the samples collected in the summer and spring seasons from inside and outside the Roman Mosaic Edifice, which exceeded the maximum admitted value of Pb concentration in the air, 0.7 mg/kg (Figure 4), according to the Romanian legislation. This can be explained by the fact that the maritime traffic became very heavy in the spring and summer seasons. To sum up, the elements present evidenced high four-season average concentrations (i.e., exceeded only for Pb), thus indicating that the composition of particles was strongly influenced by anthropogenic activities and sea salt.

Pearson correlation analyses for the metal concentration in PM_{2.5-10} samples as well as indoor and outdoor temperature, RH, and AT were carried out. The results of the correlation analysis are shown in Tables 5 and 6. Concerning the indoor parameters, a strong relationship was found between Cr, Ni, Cu, Cd, and Pb concentrations, temperature, and AT. Also, a high correlation was found between Al concentrations, temperature, and AT. Concerning the outdoor parameters, a weak correlation was found between Al concentrations, temperature, and AT. Also, a high correlation was found between Mn and Cu concentrations, temperature, and AT. A strong relationship was found between Cr, Fe, Ni, Zn, Cd, and Pb concentrations, temperature, and AT.

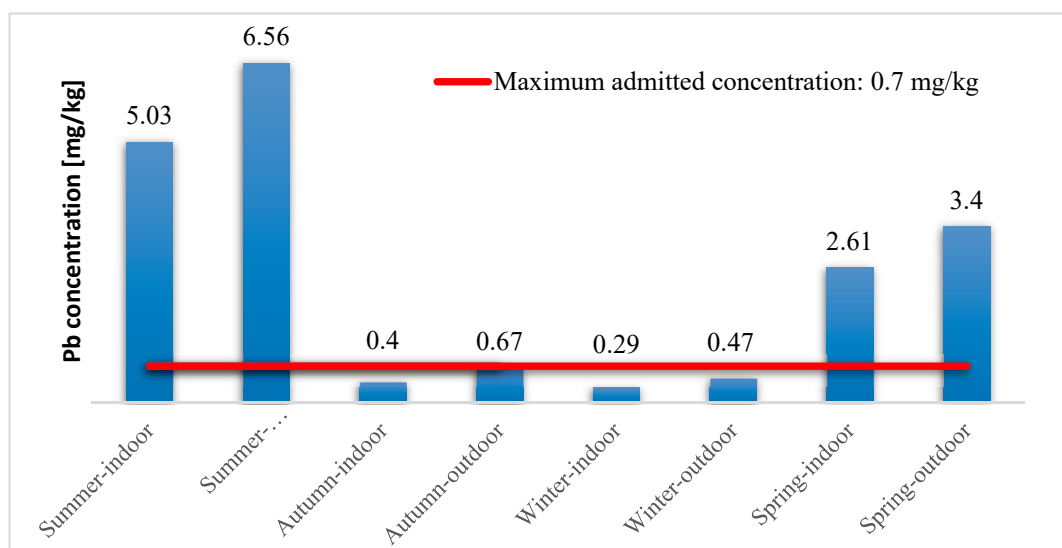


Figure 4. Pb concentrations in PM_{2.5-10} samples compared with the maximum admitted concentration in the air, according to the Romanian legislation.

Table 5. Pearson correlation coefficients between metal concentrations and indoor temperature, RH, and AT.

Parameter	Al	Cr	Mn	Fe	Ni	Cu	Zn	Cd	Pb	T (°C)	RH (%)	AT (°C)
Al indoor	1	0.93	−0.34	0.72	0.95 *	0.94	−0.30	0.91	0.93	0.87	−0.35	0.87
Cr indoor	0.93	1	−0.04	0.44	0.99 **	0.99 **	−0.03	0.99 **	0.99 **	0.98 *	−0.11	0.98 *
Mn indoor	−0.34	−0.04	1	−0.70	−0.19	−0.12	0.99 **	−0.04	−0.11	0.12	0.28	0.12
Fe indoor	0.72	0.44	−0.70	1	0.48	0.45	−0.61	0.37	0.43	0.34	−0.79	0.34
Ni indoor	0.95 *	0.99 **	−0.15	0.48	1	0.99 **	−0.15	0.99 **	0.99 **	0.95 *	−0.08	0.95 *
Cu indoor	0.94	0.99 **	−0.12	0.45	0.99 **	1	−0.12	0.99 **	0.99 **	0.96 *	−0.06	0.96 *
Zn indoor	−0.30	−0.03	0.99 **	−0.61	−0.15	−0.12	1	−0.04	−0.11	0.14	0.14	0.14
Cd indoor	0.91	0.99 **	−0.04	0.37	0.99 **	0.99 **	−0.04	1	0.99 **	0.97 *	0.01	0.97 *
Pb indoor	0.93	0.99 **	−0.11	0.43	0.99 **	0.99 **	−0.11	0.99 **	1	0.96 *	−0.03	0.96 *
T [°C] indoor	0.87	0.98 *	0.12	0.34	0.95 *	0.96 *	0.14	0.97 *	0.96 *	1	−0.10	0.99 **
RH [%] indoor	−0.35	−0.11	0.28	−0.79	−0.08	−0.06	0.14	0.01	−0.03	−0.10	1	−0.10
AT [°C] indoor	0.87	0.98 *	0.12	0.34	0.95 *	0.96 *	0.14	0.97 *	0.96 *	0.99 **	−0.10	1

Significance level, p : * < 0.05; ** < 0.01.

Table 6. Pearson correlation coefficients between metals concentrations and outdoor temperature, RH and AT.

Parameter	Al	Cr	Mn	Fe	Ni	Cu	Zn	Cd	Pb	T (°C)	RH (%)	AT (°C)
Al outdoor	1	0.78	0.88	0.84	0.86	0.87	0.83	0.82	0.86	0.57	−0.16	0.57
Cr outdoor	0.78	1	0.98 *	0.99 *	0.98 *	0.98 *	0.99 **	0.99 **	0.98 *	0.94	−0.66	0.94
Mn outdoor	0.88	0.98 *	1	0.99 **	0.99 **	0.99 **	0.99 **	0.99 **	0.99 **	0.88	−0.57	0.88
Fe outdoor	0.84	0.99 *	0.99 **	1	0.99 **	0.99 **	0.99 **	0.99 **	0.99 **	0.92	−0.63	0.92
Ni outdoor	0.86	0.98 *	0.99 **	0.99 **	1	0.99 **	0.99 **	0.99 **	0.99 **	0.90	−0.60	0.90
Cu outdoor	0.87	0.98 *	0.99 **	0.99 **	0.99 **	1	0.99 **	0.99 **	0.99 **	0.89	−0.59	0.89
Zn outdoor	0.83	0.99 **	0.99 **	0.99 **	0.99 **	0.99 **	1	0.99 *	0.99 **	0.92	−0.64	0.92
Cd outdoor	0.82	0.99 **	0.99 **	0.99 **	0.99 **	0.996 **	0.99 **	1	0.99 **	0.92	−0.64	0.92
Pb outdoor	0.86	0.98 *	0.99 **	0.99 **	0.99 **	0.99 **	0.99 **	0.99 **	1	0.90	−0.62	0.91
T [°C] outdoor	0.57	0.94	0.88	0.92	0.90	0.89	0.92	0.92	0.90	1	−0.87	0.99 **
RH [%] outdoor	−0.16	−0.66	−0.57	−0.63	−0.60	−0.59	−0.64	−0.64	−0.62	−0.87	1	−0.87
AT [°C] outdoor	0.57	0.94	0.88	0.92	0.90	0.89	0.92	0.92	0.91	0.99 **	−0.87	1

Significance level, p : * < 0.05; ** < 0.01.

Previous research highlights the fact that the elements mostly concentrated in the accumulation mode are S, As (with chemical speciation), Se, Ag, Cd, Tl, and Pb, while the elements having multimode distributions are Be, Na, K, Cr, Mn, Co, Ni, Cu, Zn, Ga, Mo, Sn, and Sb [5,23,24]. Previous studies have highlighted the relationship between metal compositions and functional groups from PM_{2.5–10} in different sizes [5,23,24,26,38–40]. In this respect, the presence of sulfate, carbonate, ammonium, and nitrate groups, as well as of organic functional groups such as aliphatic carbons, carbonyls, and organic nitrates in PM_{2.5–10} samples, collected during a complete seasonal cycle was identified by the non-destructive ATR-FTIR technique, as shown by the data presented in Tables 7 and 8. Based on FTIR spectra, the molecular characteristics in PM_{2.5–10} were examined as well as the changes in chemical composition under the influence of temperature, RH, and different oxidizing processes. FTIR spectra were acquired rapidly and non-destructively from PTFE filters, which are commonly used for gravimetric mass analysis in regulatory monitoring. After the correction for the background spectrum was made, all the spectra analyzed showed weak and medium vibrational frequencies (Tables 7 and 8) around 615 and 1130 cm^{−1} for SO₄^{2−} ions. The weak and medium peaks around 820 and 1360 cm^{−1} were assigned to NO₃[−] ions, with those above 1460 cm^{−1} corresponding to NH₄⁺ cations. The strong signals around 712 cm^{−1} were attributed to geogenic CO₃^{2−} ions, derived from local carbonate rocks.

Table 7. Tentative assignments of significant peaks from FTIR spectra; S1–S7 represents PM samples collected in the summer season; A1–A7 represents PM_{2.5–10} samples collected in the autumn season; both sets of samples were measured inside the Roman Mosaic Edifice area.

Summer of 2018							Autumn of 2018							Assignment
S1	S2	S3	S4	S5	S6	S7	A1	A2	A3	A4	A5	A6	A7	
Wavenumber [cm ^{−1}] & Relative Intensity *														
3362w	3363w	3362w	3365w	3361w	3369w	3367w	3365m	3357m	3361m	3363m	3356m	3361m	3363m	stretching O–H
1792w	1793w	1796w	1795w	-	1796w	1794w	1791w	1795w	-	1795w	1798w	1790w	1792w	C–O (CO ₃ ^{2−})
-	1632m	-	-	1639m	-	-	1637m	1639m	1647s	1635s	1629m	1635m	1639m	C–NH ₂ (amine)
1465m	1463s	1465m	1465m	1462m	1464m	1461m	1463s	1461s	1462s	1460m	1462m	1465m	1463m	N–H (NH ₄ ⁺) and C–O (CO ₃ ^{2−})
1393s	-	1391s	1392s	1393s	1408s	-	-	-	-	-	1395s	1392s	1394s	C–O (CO ₃ ^{2−})
1363m	1368m	1368m	1364m	1361m	1360m	1363m	1367m	1362w	1365w	1365w	1364m	1361m	1367m	N–O (NO ₃ [−])
1131m	1130m	1138m	1127m	1130m	1123m	1132m	1127m	1128w	1130m	1122w	1123m	1127w	1129m	S–O (SO ₄ ^{2−})
1040s	1043s	1035s	1040s	1036m	1042m	1035m	1038m	1039m	1041m	1039m	1037m	1038m	1040m	Si–O (SiO ₄ ^{4−})
870s	874s	875s	876m	873s	873s	873s	873s	873s	873s	872s	872s	872s	871s	C–O (CO ₃ ^{2−})
820w	817w	825w	821w	823w	823w	821w	818w	821w	819w	822w	-	820w	-	N–O (NO ₃ [−])
796m	794m	797m	794m	795m	800m	796m	796w	797w	-	-	-	-	-	Si–O (quartz)
781s	781s	778s	777s	780s	778m	781m	778w	780w	-	-	-	-	-	Si–O (quartz)
711s	712s	713s	712s	712m	712s	712s	712s	711s	712m	712s	713s	712s	712s	Ca–O (CaCO ₃)
618w	614w	614w	616w	615w	618w	612w	615w	614w	617w	615w	612w	616w	610w	S–O (SO ₄ ^{2−})
465m	-	461w	469w	465w	464w	-	460s	-	-	-	467w	-	-	Si–O (SiO ₄ ^{4−})
431w	444s	439w	439s	445s	443w	-	447w	-	445w	-	431w	-	445w	Si–O (SiO ₄ ^{4−})
-	-	427w	-	-	420w	426w	-	-	429w	-	-	-	429w	Ti–O (rutile)
406m	412m	416m	402m	417m	400m	414w	-	398s	390s	399m	-	398m	394s	Si–O (quartz)

* s—strong; m—medium; w—weak.

Table 8. Tentative assignments of significant peaks from FTIR spectra; W1–W7 represents PM samples collected in the winter season; Sp1–Sp7 represents PM_{2.5–10} samples collected in summer and spring; both sets of samples were measured inside the Roman Mosaic Edifice area.

Winter of 2018 to 2019							Spring of 2019							Assignment
W1	W2	W3	W4	W5	W6	W7	Sp1	Sp2	Sp3	Sp4	Sp5	Sp6	Sp7	
Wavenumber [cm ^{−1}] & Relative Intensity *														
3362w	3363w	3362w	3365w	3361w	3369w	3367w	3360m	3361m	3363m	3361w	3360w	3361w	3360w	stretching O–H
1793w	1795w	1796w	-	-	1796w	1794w	1794w	1792w	1790w	1790w	1794w	1795w	1791w	C–O (CO ₃ ^{2−})
-	-	-	-	1632s	-	-	-	1635s	-	1634s	1630s	1633s	-	C–NH ₂ (amine)
1465s	1463s	1465s	1465s	1462s	1464s	1461s	1461s	1464s	1465s	1463s	1463s	1462s	1465s	N–H (NH ₄ ⁺) and C–O (CO ₃ ^{2−})
1395s	-	1396s	1397s	1397s	1398s	-	1392s	-	-	-	1390s	1391s	1392s	C–O (CO ₃ ^{2−})
1363m	1364m	1365m	1363m	1361m	1361m	1362m	1365w	1363w	1364w	1365w	1362w	1364w	1363w	N–O (NO ₃ [−])
1131m	1130m	1138m	1127w	1130m	1123m	1132w	1127w	1128w	1128w	1127w	1123w	1127w	1129w	S–O (SO ₄ ^{2−})
1040m	1043m	1039m	1040m	1039m	1040m	1038m	1039s	1039s	1040s	1039s	1038s	1040s	1039m	Si–O (SiO ₄ ^{4−})
872s	872s	873s	872s	872s	871s	870s	875s	874s	878s	876m	879s	875s	875s	C–O (CO ₃ ^{2−})
820w	-	-	820w	-	820w	-	823w	822w	825w	821w	823w	824w	825w	N–O (NO ₃ [−])
-	797w	-	-	-	-	-	795m	792m	793m	794m	792m	796m	795m	Si–O (quartz)
779w	-	-	-	-	-	-	781s	780s	780s	782s	781s	781m	-	Si–O (quartz)
712w	712m	712m	711w	712w	711w	710w	711s	712s	713s	712s	712m	712s	712s	Ca–O (CaCO ₃)
612w	612w	615w	615w	612w	615w	612w	618w	614w	614w	616w	615w	618w	612w	S–O (SO ₄ ^{2−})
460s	-	-	-	467w	-	-	465m	-	-	469w	465w	464w	-	Si–O (SiO ₄ ^{4−})
446w	-	446w	-	-	-	-	431w	444s	439w	439s	445s	443w	-	Si–O (SiO ₄ ^{4−})
-	-	429w	-	-	-	-	-	-	429w	-	-	-	-	Ti–O (rutile)
-	395s	397s	396m	-	398m	396s	406m	412m	416m	402m	417m	400m	414w	Si–O (quartz)

* s—strong; m—medium; w—weak.

Vibrational assignments around 870, 1395, 1465, and 1792 cm^{-1} corresponded to CO_3^{2-} ions as well. Silicate, SiO_4^{4-} ions, identified by the weak, medium, or strong peaks around 439, 465, and 1040 cm^{-1} , respectively, were detected mainly in samples collected in the summer of 2018 and spring of 2019 (Table 8). The medium or strong peaks around 400 cm^{-1} and 777–797 cm^{-1} were attributed to Si-O from quartz, which was present in all samples. FTIR also identified several organic functional groups, although specific organic molecules could not be identified. The broad bands in the region 3357–3367 cm^{-1} were assigned to OH-stretching mainly from water. In conclusion, the ions distribution in $\text{PM}_{2.5-10}$ highlighted several main peaks for NO_3^- , CO_3^{2-} , SO_4^{2-} , SiO_4^{4-} , and NH_4^+ groups as well as for organic carbon (i.e., amines, carbonyl compounds) as a major part of the particle mass. In addition, the $\text{PM}_{2.5-10}$ mass composition highlighted the fact that ions and organic compounds constituted a major part of the particulate matter, while metals and other substances constituted the remaining particle mass. Statistical analysis showed that the chemical composition of particulate matter examined in the indoor and outdoor areas of the Roman Mosaic Edifice was influenced by microclimatic conditions, mainly temperature and RH.

4. Conclusions

The final results allowed an estimation of indoor and outdoor air quality, from the point of view of the PM chemical composition, thus giving insight into the health risks for visitors and within the Roman Mosaic Edifice museum space hosted in buildings with natural ventilation. The particulate matter analyses showed variability related to indoor microclimate conditions as well as to outdoor, coastal anthropic activities. The FTIR and ICP-MS techniques, used for the investigation of $\text{PM}_{2.5-10}$ samples, revealed high concentrations of Fe, Al-rich, and soluble particles inside the investigated museum area. The high values of the measured RH in outdoor areas (99% in the monitoring process in the autumn of 2018 and spring of 2019, and over 50% in the indoor area in all seasons), correlated with the temperature and influenced the chemical composition of $\text{PM}_{2.5-10}$ samples. A strong relationship was found between Cr, Ni, Cu, Cd, and Pb concentrations, temperature, and AT inside the Roman Mosaic Edifice area. On the other hand, a high correlation was found between Al concentrations, temperature, and AT. A low correlation was observed between Al concentrations, temperature, and AT in the outdoor area of the Roman Mosaic Edifice as well as a high correlation between Mn and Cu concentrations, temperature, and AT. In this respect, a strong relationship was remarked between Cr, Fe, Ni, Zn, Cd, and Pb concentrations, temperature, and AT inside the investigated area. The order of the metals analyzed in terms of their abundance in the cold seasons (i.e., autumn and winter, when the temperatures ranged between 0 °C and 10 °C), inside and outside the investigated area, were found to be the same. However, the rise in temperature led to a change in the order of the metals inside the Roman Mosaic Edifice area. The data obtained indicated that as the temperature increases (i.e., in the summer and spring seasons), the Pb concentrations both inside and outside the investigated area are much higher than expected, mainly because of the anthropic activities conducted in the port of Constanta. In conclusion a confined outdoor environment may not be suitable for the conservation of original heritage materials, depending on the climatic region. Several solutions will be proposed in the future, at the end of the project, in order to reduce the impact of the external climatic risk and the consequences of the thermo-hygrometric variations inside the museum, which may have harmful effects on the historical materials and the visitors' health.

Author Contributions: C.R. and C.S. contributed equally to the work; Conceptualization, C.R. and C.S.; Funding acquisition, C.R., and R.-M.I.; Investigation, I.-D.D., R.M.S., S.T., D.-D.L., L.O., I.-V.G., N.-M.S., C.-M.N., I.-A.B., and R.-L.O.; Methodology, C.R., C.S., and I.-D.D.; Project administration, C.R. and R.-M.I.; Software, S.-G.S. and C.S.; Supervision, C.R. and C.S.; Writing—original draft preparation, C.R. and C.S.; Writing—reviewing and editing, C.R., C.S., and S.-G.S.

Funding: This research was funded by the Romanian National Authority for Scientific Research, UEFISCDI, project 51PCCDI/2018 “New diagnosis and treatment technologies for the preservation and revitalization of the archaeological components of the national cultural heritage”.

Conflicts of Interest: The authors declare no conflicts of interest.

References

- Kim, K.H.; Kabir, E.; Kabir, S. A review on the human health impact of airborne particulate matter. *Environ. Int.* **2015**, *74*, 136–143. [CrossRef] [PubMed]
- Saenz-de-Miera, O.; Rossello, J. Modeling tourism impacts on air pollution: The case study of PM10 in Mallorca. *Tour. Manag.* **2014**, *40*, 273–281. [CrossRef]
- Zwozdziak, A.; Sówka, I.; Willak-Janc, E.; Zwozdziak, J.; Kwiecińska, K.; Balińska-Miśkiewicz, W. Influence of PM 1 and PM 2.5 on lung function parameters in healthy schoolchildren—A panel study. *Environ. Sci. Pollut. Res.* **2016**, *23*, 23892–23901. [CrossRef] [PubMed]
- Dunea, D.; Iordache, S.; Liu, H.Y.; Böhler, T.; Pohoata, A.; Radulescu, C. Quantifying the impact of PM 2.5 and associated heavy metals on respiratory health of children near metallurgical facilities. *Environ. Sci. Pollut. Res.* **2016**, *23*, 15395–15406. [CrossRef] [PubMed]
- Radulescu, C.; Iordache, S.; Dunea, D.; Stihl, C.; Dulama, I.D. Risks assessment of heavy metals on public health associated with atmospheric exposure to PM2. 5 in urban area. *Rom. J. Phys.* **2015**, *60*, 1171–1182.
- World Health Organisation. Ambient Air Pollution: A Global Assessment of Exposure and Burden of Disease. 2016. Available online: <http://www.who.int/iris/bitstream/handle/10665/250141/9789241511353-eng.pdf> (accessed on 5 July 2019).
- Pope, C.A.; Burnett, R.T.; Thun, M.J.; Calle, E.E.; Krewski, D.; Ito, K.; Thurston, G.D. Lung cancer, cardiopulmonary mortality, and long-term exposure to fine particulate air pollution. *JAMA* **2002**, *287*, 1132–1141. [CrossRef] [PubMed]
- Beelen, R.; Hoek, G.; van den Brandt, P.A.; Goldbohm, R.A.; Fischer, P.; Schouten, L.J.; Jerrett, M.; Hughes, E.; Armstrong, B.; Brunekreef, B. Long-term effects of traffic-related AIR pollution on mortality in a Dutch cohort (NLCS-AIR study). *Environ. Health Perspect.* **2008**, *116*, 196–202. [CrossRef] [PubMed]
- Raaschou-Nielsen, O.; Andersen, Z.J.; Beelen, R.; Samoli, E.; Stafoggia, M.; Weinmayr, G.; Hoffmann, B.; Fischer, P.; Nieuwenhuijsen, M.J.; Brunekreef, B.; et al. Air pollution and lung cancer incidence in 17 European cohorts: Prospective analyses from the European Study of Cohorts for Air Pollution Effects (ESCAPE). *Lancet Oncol.* **2013**, *14*, 813–822. [CrossRef]
- Sett, R. Responses in plants exposed to dust pollution. *Hortic. Int. J.* **2017**, *1*, 1–5. [CrossRef]
- Honour, S.L.; Bell, J.N.B.; Ashenden, T.W.; Cape, J.N.; Power, S.A. Responses of herbaceous plants to urban air pollution: Effects on growth, phenology and leaf surface characteristics. *Environ. Pollut.* **2009**, *157*, 1279–1286. [CrossRef]
- Poudyal, N.C.; Paudel, B.; Green, G.T. Estimating the impact of impaired visibility on the demand for visits to national parks. *Tour. Econ.* **2013**, *19*, 433–452. [CrossRef]
- Kroeger, T.; McDonald, R.I.; Boucher, T.; Zhang, P.; Wang, L. Where the people are: Current trends and future potential targeted investments in urban trees for PM10 and temperature mitigation in 27 US cities. *Landsc. Urban Plan* **2018**, *177*, 227–240. [CrossRef]
- Camuffo, D.; Van Grieken, R.; Busse, H.J.; Sturaro, G.; Valentino, A.; Bernardi, A.; Blades, N.; Shooter, D.; Gysels, K.; Deutsch, F.; et al. Environmental monitoring in four European museums. *Atmos. Environ.* **2001**, *35*, 127–140. [CrossRef]
- Godoi, R.H.M.; Potgieter-Vermaak, S.; Godoi, A.F.L.; Stranger, M.; Van Grieken, R. Assessment of aerosol particles within the Rubens' House Museum in Antwerp, Belgium. *X-RAY Spectrom.* **2008**, *37*, 298–303. [CrossRef]
- Matus, K.; Nam, K.M.; Selin, N.E.; Lamsa, L.N.; Reilly, J.M.; Paltsev, S. Health damages from air pollution in China. *Glob. Environ. Chang.* **2012**, *22*, 55–66. [CrossRef]
- Pascal, M.; Falq, G.; Wagner, V.; Chatignoux, E.; Corso, M.; Blanchard, M.; Host, S.; Pascal, L.; Larrieu, S. Short-term impacts of particulate matter (PM10, PM10–2.5, PM2. 5) on mortality in nine French cities. *Atmos. Environ.* **2014**, *95*, 175–184. [CrossRef]
- Brimblecombe, P. The composition of museum atmospheres. *Atmos. Environ. B Urban Atmos.* **1990**, *24*, 1–8. [CrossRef]
- Chianese, E.; Riccio, A.; Duro, I.; Trifuoggi, M.; Iovino, P.; Capasso, S.; Barone, G. Measurements for indoor air quality assessment at the Capodimonte Museum in Naples (Italy). *Int. J. Environ. Resour.* **2012**, *6*, 509–518.

20. Ion, R.M.; Iancu, L.; Vasilievici, G.; Grigore, M.E.; Andrei, R.E.; Radu, G.I.; Grigorescu, R.M.; Teodorescu, S.; Bucurica, I.A.; Ion, M.L.; et al. Ion-Substituted Carbonated Hydroxyapatite Coatings for Model Stone Samples. *Coatings* **2019**, *9*, 231. [[CrossRef](#)]
21. Maddison, D. In search of warmer climates? The impact of climate change on flows of British tourists. *Clim. Chang.* **2001**, *49*, 193–208. [[CrossRef](#)]
22. Serafima, S.; Duliu, O.G.; Manea, M.M.; Vasilica, S.; Radulescu, C.; Constantinescu, B.; Stan, D.; Culicov, O.A.; Zincovscaia, I. Complex investigation of the five 19th century Russian-Lipovan icons. *Microchem. J.* **2019**, in press. [[CrossRef](#)]
23. Radulescu, C.; Stih, C.; Dulama, I.D. Chapter 4: Elemental analysis methods for particulate matter. Chemical speciation. Analytical method validation. In *Methods for the Assessment of Air Pollution with Particulate Matter to Children's Health*; Iordache, S., Dunea, D., Eds.; MatrixRom: Bucharest, Romania, 2014; pp. 119–187.
24. Radulescu, C.; Stih, C.; Iordache, S.; Dunea, D.; Dulama, I.D. Characterization of urban atmospheric PM_{2.5} by ATR-FTIR, ICP-MS and SEM-EDS techniques. *Rev. Chim. Buchar.* **2017**, *68*, 805–810.
25. Spolnik, Z.; Worobiec, A.; Injuk, J.; Neilen, D.; Schellen, H.; Van Grieken, R. Chemical characterization of airborne particles in St. martinus cathedral in Weert, The Netherlands. *Microchim. Acta* **2004**, *145*, 223–227.
26. Iordache, S.; Dunea, D.; Radulescu, C.; Dulama, I.D.; Ianache, R.; Predescu, M. Investigation of Heavy Metals Content in Airborne Particles from Ploesti, Romania. *Rev. Chim. Buchar.* **2017**, *68*, 879–885.
27. Spolnik, Z.; Worobiec, A.; Samek, L.; Bencs, L.; Belikov, K.; Van Grieken, R. Influence of different types of heating systems on particulate air pollutant deposition: The case of churches situated in a cold climate. *J. Cult. Herit.* **2007**, *8*, 7–12. [[CrossRef](#)]
28. Grau-Bové, J.; Strlič, M. Fine particulate matter in indoor cultural heritage: A literature review. *Herit. Sci.* **2013**, *1*, 8. [[CrossRef](#)]
29. *Guidebook*; Museum of National History and Archaeology: Constanta, Romania, 1979.
30. Lee, K.; Lee, D. The relationship between indoor and outdoor temperature in two types of residence. *Energy Proc.* **2015**, *78*, 2851–2856. [[CrossRef](#)]
31. Radulescu, C.; Olteanu, R.L.; Stih, C.; Florescu, M.; Lazurca, D.; Dulama, I.D.; Stirbescu, R.M.; Teodorescu, S. Chemometric Assessment of Spectroscopic Techniques and Antioxidant Activity for Hippophae rhamnoides L. Extracts Obtained by Different Isolation Methods. *Anal. Lett.* **2019**, *52*, 2393–2415. [[CrossRef](#)]
32. Buruleanu, L.; Radulescu, C.; Georgescu, A.A.; Dulama, I.D.; Nicolescu, M.C.; Olteanu, R.L.; Stanescu, S.G. Chemometric Assessment of the Interactions between the Metal Contents, Antioxidant Activity, Total Phenolics, and Flavonoids in Mushrooms. *Anal. Lett.* **2019**, *52*, 1195–1214. [[CrossRef](#)]
33. Buruleanu, L.; Radulescu, C.; Georgescu, A.A.; Danet, A.F.; Olteanu, R.L.; Nicolescu, M.C.; Dulama, I.D. Statistical Characterization of the Phytochemical Characteristics of Edible Mushroom Extracts. *Anal. Lett.* **2018**, *51*, 1039–1059. [[CrossRef](#)]
34. Radulescu, C.; Pohoata, A.; Bretcan, P.; Tanislav, D.; Stih, C.; Chelarescu, E.D. Quantification of major ions in groundwaters using analytical techniques and statistical approaches. *Rom. Rep. Phys.* **2017**, *69*, 705–717.
35. Ferdyn-Grygierek, J. Monitoring of indoor air parameters in large museum exhibition halls with and without air-conditioning systems. *Build. Environ.* **2016**, *107*, 113–126. [[CrossRef](#)]
36. McMullan, R. *Environmental Science in Building*, 7th ed.; Basingstoke: Houndmills, UK; Palgrave Macmillan: New York, NY, USA, 2012; p. 25.
37. Nguyen, J.L.; Schwartz, J.; Dockery, D.W. The relationship between indoor and outdoor temperature, apparent temperature, relative humidity, and absolute humidity. *Indoor Air* **2014**, *24*, 103–112. [[CrossRef](#)] [[PubMed](#)]
38. Bintintan, A.; Gligor, M.; Radulescu, C.; Dulama, I.D.; Olteanu, R.L.; Teodorescu, S.; Stirbescu, R.M.; Bucurica, I.A. Multielemental and Chemical Characterization of Eneolithic Petresti Painted Pottery from Alba Iulia-Lumea Noua archaeological site, Romania. *Anal. Lett.* **2019**, *52*, 2348–2364. [[CrossRef](#)]

39. Radulescu, C.; Bucurica, I.A.; Bretcan, P.; Chelarescu, E.D.; Tanislav, D.; Dulama, I.D.; Stirbescu, R.M.; Teodorescu, S. Complex Investigation of Unconsolidated Sediments of Romanian Plain Salt Lake. *Rom. J. Phys.* **2019**, *64*, 809.
40. Pehoiu, G.; Radulescu, C.; Murarescu, O.; Dulama, I.D.; Bucurica, I.A.; Teodorescu, S.; Stirbescu, R.M. Health risk assessment associated with abandoned copper and uranium mine tailings. *Bull. Environ. Contam. Toxicol.* **2019**, *102*, 504–510. [[CrossRef](#)] [[PubMed](#)]



© 2019 by the authors. Licensee MDPI, Basel, Switzerland. This article is an open access article distributed under the terms and conditions of the Creative Commons Attribution (CC BY) license (<http://creativecommons.org/licenses/by/4.0/>).